Geophysical Journal International

Geophys. J. Int. (2010) **183,** 681–694 doi: 10.1111/j.1365-246X.2010.04789.x

Electric pore fabric of the Nubia sandstones in south Egypt: characterization and modelling

Bassem S. Nabawy,[1,2] Pierre Rochette[3] and Yves Géraud[4]

[1]*Department of Geophysical Sciences, National Research Center, Cairo, Egypt. E-mail: bsnabawy@yahoo.co.uk*
[2]*Laboratoire de Géologie, Ecole Normale Supérieur, Paris, France*
[3]*CEREGE, Aix-Marseille Université, CNRS, France*
[4]*Institute de Physique du Globe, Université de Louis Pasteur, Strasbourg, France*

Accepted 2010 August 23. Received 2010 August 9; in original form 2010 January 19

SUMMARY

This study testifies the reliability of the electric pore fabric technique applied on the Nubia sandstones in south Egypt through a comparison with pre-assigned magnetic pore fabric and permeability already measured for three perpendicular directions in these rocks. Discrepancies between the different techniques were attributed to the fact that the magnetic pore fabric technique has the ability to detect and define accurately the pore volume distribution in 3-D, whereas the electric pore fabric technique has the ability to detect the shortest paths for the electric current/fluid flow. Although the magnetic pore fabric is a bulk property, the permeability measurements and the electric pore fabric are quantifying transport properties.

Both the magnetic and electric pore fabrics refer mostly to slightly and moderately anisotropic fabrics. The integration between both techniques revealed two main directions for fluid migration, swinging to the N–S and the E–W directions.

One difficulty of the electric pore fabric technique is due to the surface conductivity effects either from the presence of some clay minerals or cracks. Therefore, interpreting the obtained electric pore fabric must be carried out in care for the cracked and clayey rocks. The surface conductivity effect could be accounted for by using the true formation factor for calculating the electric pore fabric parameters.

The electric pore fabric technique can be compared to the 3-D permeability measurements, which show very similar directions.

Key words: Magnetic and electrical properties; Magnetic fabrics and anisotropy; Permeability and porosity.

1 INTRODUCTION

Determining porosity and permeability is a main target for those interested in natural resources, especially fluids such as ground water and oil and gas. Quantifying permeability anisotropy is of course an important problem related to fluid extraction from the Earth.

The Anisotropy of Magnetic Susceptibility (AMS or magnetic fabric) has been found to generally provide a good estimate of petrofabric 'it is the preferred alignment of grains in the rock fabric' (e.g. Tarling & Hrouda 1993). AMS is sensitive to changes in petrofabric and can therefore be used successfully as a tool of petrofabric and structural analysis. Due to measurement speed, precision, low cost and range of applicability, AMS has gained a widespread use in petrofabric studies of rocks (Hrouda 1982; Tarling & Hrouda 1993). In particular, directions of the principal susceptibility axes ($\chi_{\max}$) and sedimentary structures have been found to be in good agreement (Hamilton & Rees 1970); therefore, AMS can be used in the investigation of palaeocurrents in sedimentation basins. Moreover, pore orientation and shape can be determined using magnetic pore fabric analysis (Pfleiderer & Kissel 1994). Connected pores can be injected with a magnetic suspension (ferrofluid) then measured for AMS. The maximum susceptibility of the pore fabric is parallel to the preferred directions of pore elongation. Any anisotropic shape of pore bodies will also cause AMS.

Rock electrical resistivity is another physical property of great interest. For a porous saturated rock, electric current is carried by the fluid phase. The resistivity of porous rocks is controlled mainly by (1) the pore phase (its volume, geometry and distribution) and (2) the resistivity of saline solution within the pore spaces. In fact, the resistivity 'R_O' of saturated porous sedimentary rocks is mainly of electrolytic origin, because resistivity of the solid matrix is much larger than that of the saline solution 'R_f'. The apparent formation resistivity factor 'F_a' has been defined by many workers (e.g. Archie 1942; Amyx *et al.* 1960; Serra 1984) using the following equation:

$$F_a = R_O/R_f. \quad (1)$$

The true formation factor 'F' can be obtained by applying the following equation (Lamb 1945; Worthington 1985; Mavco *et al.* 2009):

$$\sigma_r = \frac{1}{F}\sigma_f + \sigma_s, \tag{2}$$

where, σ_f and σ_r are the electric conductivity of the saturating fluid and the measured rock, respectively, whereas σ_s is the surface conductivity of the pore walls.

A large number of measurements have demonstrated that the formation resistivity factor (F) of clean rocks is related to the connected porosity (Archie 1942; Serra 1984) as follows:

$$F = a/\emptyset^m, \tag{3}$$

where, 'a' is the lithology factor (0.6–2.0), 'm' is the cementation exponent (1.0–3.0) and ø is the porosity (0.0–1.0).

Many authors such as Archie (1942), Amyx *et al.* (1960), Lynch (1962) and Serra (1984) discussed the variation of 'a' and 'm' and attributed them to (1) degree of cementation, (2) pore geometry and tortuosity, (3) type of clay minerals and distribution, (4) presence of conductive solids and (5) compaction and packing. Recently, Salem & Chilingarian (1999) confirmed that the cementation exponent (m) of Archie's equation is not a constant, but varies with many physical parameters and lithological attributes. It depends on the shape, type and size of pore throats and the size and number of the dead-end pores. Electrical resistivity can be anisotropic and the porous network can be simulated as a network of brine-saturated conductive pore ellipsoids. In some cases, particularly that of low-porosity rocks (<5 per cent), the electrical resistivity is mostly affected by the surface conductivity due to presence of cracks and conductive clay minerals (Nabawy & El-Hariri 2008). The electric properties of different rock types have been studied by many authors, for example, (Wyllie & Rose (1950), Winsauer *et al*. (1952), Parkhomenko (1982), Serra (1984), Olhoeft (1989) and Wilt & Alumbaugh (1998). A review article on the electric properties of Egyptian rocks has been published by Ragab *et al.* (2000). Bedding-parallel anisotropy of sedimentary rocks is caused by the load pressure and the orientation of grains resulting from depositional currents. Therefore, electrical resistivity is generally anisotropic. Horizontal resistivity (R_H) is parallel to the bedding plane whereas vertical resistivity (R_V) is perpendicular to it (Serra 1984). The anisotropy coefficient, λ_E, is a measure of the degree of electrical anisotropy, and is defined by Serra (1984) as

$$\lambda_E = (R_V/R_H)^{1/2}. \tag{4}$$

In the *a priori* expected situation of a larger vertical resistivity, λ_E is larger than one. Nabawy & El-Hariri (2008) recommended measuring the petrophysical properties of sedimentary rocks in 3-D for interpreting their physical behaviour and defining the pore elongation and the preferred paths for fluid migration. To quantify the anisotropy within the bedding plane, they proposed by analogy with the magnetic fabric parameters to define the electric lineation (L_E), electric foliation (F_E) and electric anisotropy (λ_E) parameters, based on the maximum, intermediate and minimum horizontal resistivities as follows:

$$L_E = R_{\text{int}}/R_{\text{min}}, \tag{5}$$

$$F_E = R_{\text{max}}/R_{\text{int}}, \tag{6}$$

$$\lambda_E = (R_{\text{max}}/R_{\text{min}})^{1/2}. \tag{7}$$

In this study, we attempt to determine the pore fabric parameters using true formation factor (F) to avoid the influence of the brine concentration and the surface conductivity effect that can affect the measurements of the apparent formation factor.

$$L_E = F_{\text{int}}/F_{\text{min}}, \tag{8}$$

$$F_E = F_{\text{max}}/F_{\text{int}}, \tag{9}$$

$$\lambda_E = (F_{\text{max}}/F_{\text{min}})^{1/2}. \tag{10}$$

This study is a further development of the electric fabric technique introduced by Nabawy & El-Hariri (2008). It reports and compares the electric pore fabric results with some previously published magnetic pore fabric and permeability anisotropy data for the same Nubia sandstone samples collected from south Egypt (Nabawy *et al.* 2009a, 2009b).

2 SAMPLING AND MEASURING PROCEDURE

The Nubia sandstones in south Egypt extend to the northwest of Sudan, northeast of Chad and to the southeast of Libya. These formations have been studied by many authors for decades, for example, Said (1962), Issawi (1973, 1978), Issawi & Jux (1982), Klitzsch (1979), Klitzsch & Hermina (1989), Hendriks (1987, 1988), Issawi & Osman (1993), Thabit (1994).

Following Thabit (1994) and the field observations, the Nubia sandstones between latitudes 22° 15′ and 22° 35′ N and longitudes 31° 00′ and 31° 40′ (Fig. 1) can be distinguished from top to bottom into four formations as follows:

IV. Adindan Formation (Jurassic-Valanginian)
III. Abu Simbil Formation (Valanginian-Barremian)
II. Abu Ballas Formation (Aptian-Albian)
I. Kesieba Formation (Campanian-Maastrichtian)

Kesieba Formation is separated from the underlying Abu Ballas Formation by a disconformity of regional extent caused by the removal of the Sabayia Formation during a tectonic exhumation. In general, the studied Nubia sandstone samples in south Egypt were sampled from four the formations.

The methodology and results of the magnetic and permeability measurements are described in detail in Nabawy *et al*. (2009a).

Petrographically, the studied Nubia sandstones in south Egypt are composed mainly of very fine-to-medium grained, highly fractured quartz arenites, cemented by silica cement (Fig. 2). The Nubia sequence in south Egypt has been exposed to a long history of arid conditions accompanied with deposition of oolitic ironstone beds at the top of each cycle of deposition. Detailed petrographical description and micropore throats distribution of our highly porous (20–35 per cent porosity) samples is available in Nabawy *et al*. (2009b).

For this study, a total of 19 representative block samples (∼15 × 15 × 15 cm) were collected for the purpose of electric fabric measurement. These blocks are oriented according to the bedding plane, and additionally according to the magnetic north. For investigation of the mineralogical composition, some thin sections representing the different lithological varieties were prepared and impregnated with blue dye to evaluate percentage and type of pore spaces. Thin sections were studied for mineralogical analysis using a polarized microscope and a point counter was used to evaluate the percentage

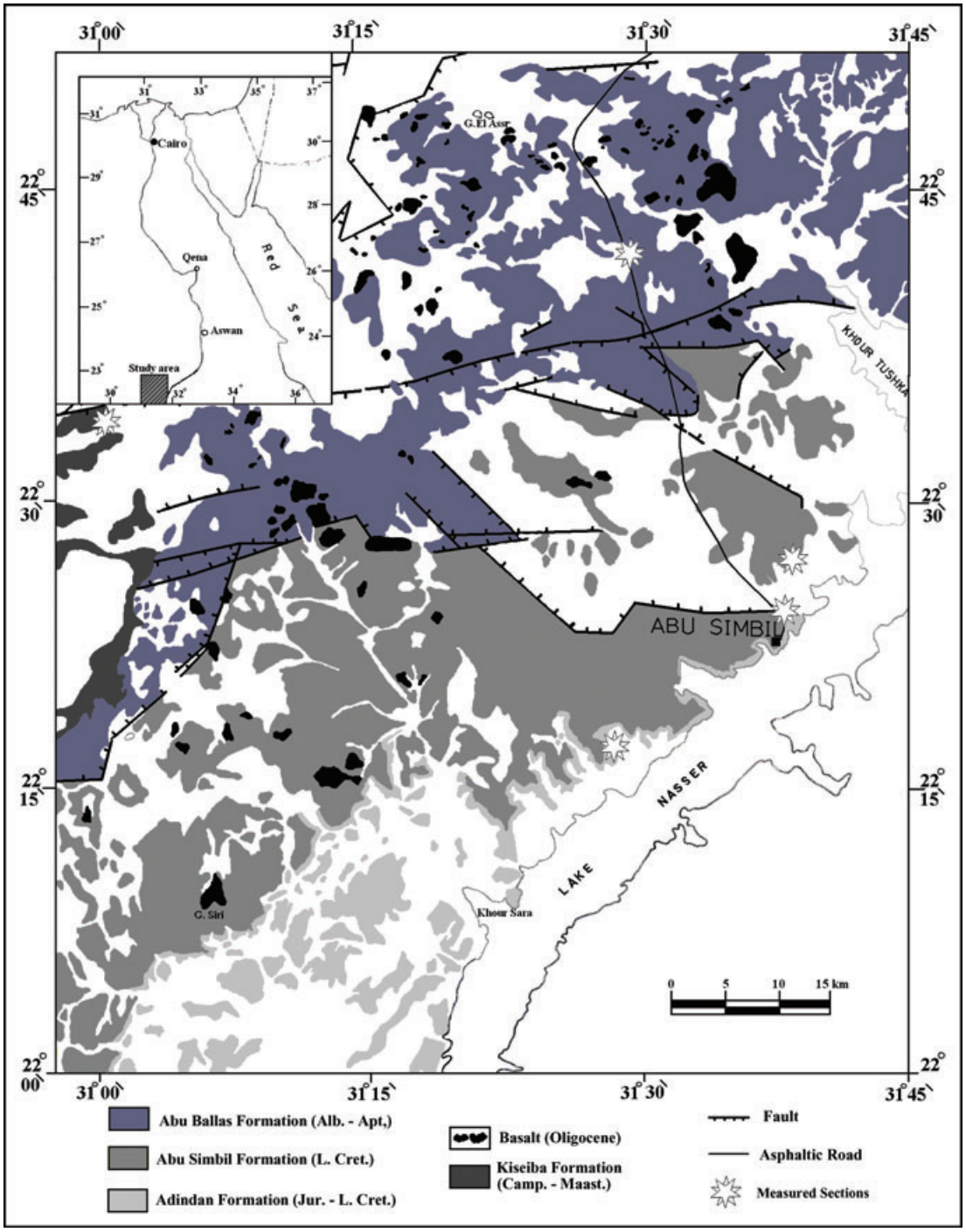

Figure 1. Location map of the studied Nubia sandstone sections in Tushka area, south of Egypt (modified from EGPC-CONOCO 1987; Thabit 1994).

of the different components. Three cubes were obtained from each block sample all with a basal face parallel to the bedding plane. The horizontal side directions of one cube refer to 0–180° and 90–270°, of another cube refer to 30–210° and 120–300° and the third cube refer to 60–240° and 150–330° (Fig. 3). Prior to measuring the electric resistivities, the studied samples were weighed dry (Wd) and evacuated in an evacuation chamber, then injected by the brine (of density $\rho_W = 1.010$ g cm^{-3}) used for the electric measurements and the samples were weighed again in the saturation state (Ws). Taking into consideration the bulk volume (Vb) of the rock sample, the connected porosity of the brine fully saturated samples ($\varnothing_W$) was calculated using the following equation:

$$\varnothing_W = 100 \times \frac{(Ws - Wd)}{Vb \times \rho_W}. \quad (11)$$

The electrical resistivity measurements of the cubic samples were carried out using a two-electrode A-C bridge at two brine concentrations (10 and 50 kppm NaCl solutions, $R_f = 0.53$ ohm.m and 0.13 ohm.m, respectively). To investigate the electric fabric for these samples, three readings along the six sides of each cube were obtained for each brine concentration, one perpendicular to the bedding plane and other two readings parallel to the bedding plane

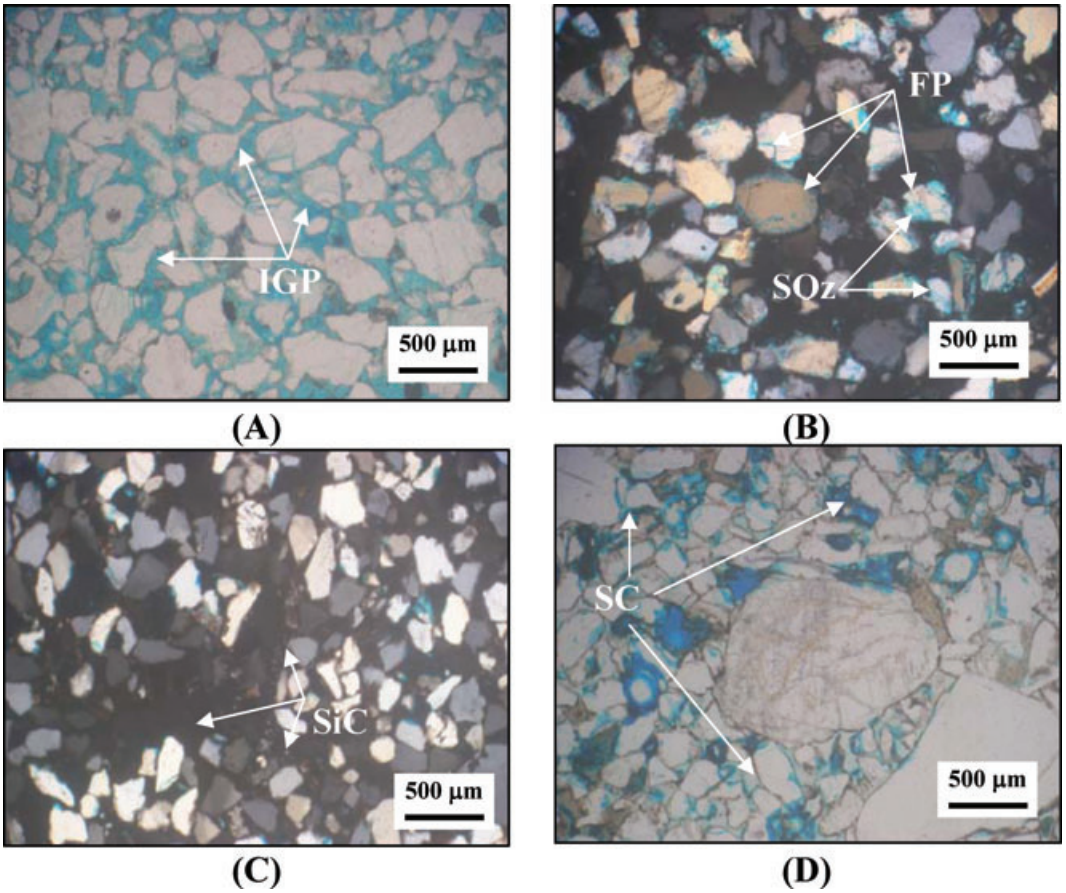

Figure 2. Photomicrographs of the Nubia sandstones in south Egypt. (A) Very fine to medium-grained quartz grains, cemented by silica cement and contain intergranular porosity (IGP), base of Abu Simbil Formation, PPL. (B) Very fine to medium-grained compacted quartz grains, fracture porosity (FP) and dissolution giving rise to exhausted skeletal quartz grains (SQz), Adindan Formation, C.N. (C) Quartz grains cemented by silica cement, Adindan Formation, C.N. (D) Fine to coarse-grained, ill sorted and angular to rounded quartz grains, sometimes are fractured with suture and point contacts (SC), Abu Ballas Formation, PPL.

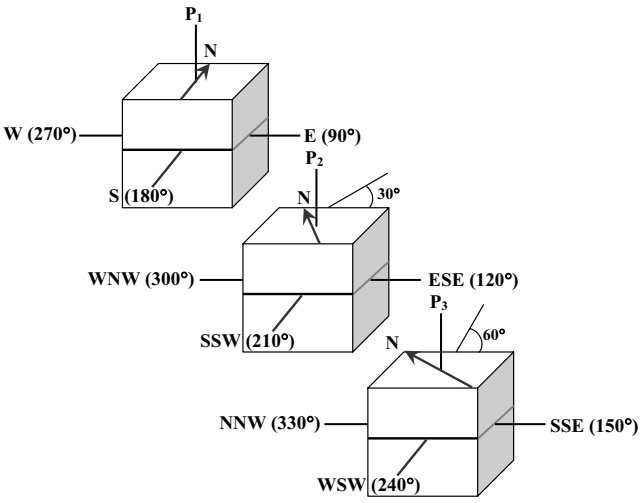

Figure 3. Three cubes out of each block sample were prepared oriented according to the bedding plane and the magnetic north, they are faced 30° clockwise.

and at 90° to each other. The electrical conductivity of the water is assumed to be homogeneous inside the sample once it is fully saturated (Jouniaux *et al.* 2006). A fixed frequency of 1 kHz was chosen for the present measurements, consistent with Glover *et al.* (1996, 1997) and Jouniaux *et al.* (2006). At this frequency, we get the best accuracy with no capacitance effect. Capacitance exists anywhere there is a conductor that is insulated from another one. At higher frequencies, the distributed capacitance in the pores reduces the signal and takes it out of the current path, that is, the higher the frequency, more signal will be lost due to this effect.

The measurements were carried out under stable ambient conditions, atmosphere and room temperature. The true formation factor '*F*' was then calculated by plotting the measured rock conductivity versus fluid conductivity (Fig. 4). We determined the true formation resistivity factor (*F*) for each of the three measured cubes/block in the direction perpendicular to the bedding plane, and horizontally parallel to the bedding plane for the six directions as defined in Fig. 3.

3 RESULTS AND ANALYSES

3.1 Magnetic pore fabric

We recall first the results obtained for the magnetic pore fabrics of the Nubia sandstone published by Nabawy *et al*. (2009a).

The magnetic pore anisotropy degree 'λ_M' (as defined by Balsley & Buddington 1960) varies from 1.017 to 1.036 (1.7–3.6 per cent), the magnetic pore lineation 'L_M' (as defined by Stacey *et al.* 1960) varies from 1.002 to 1.010, whereas the magnetic pore foliation

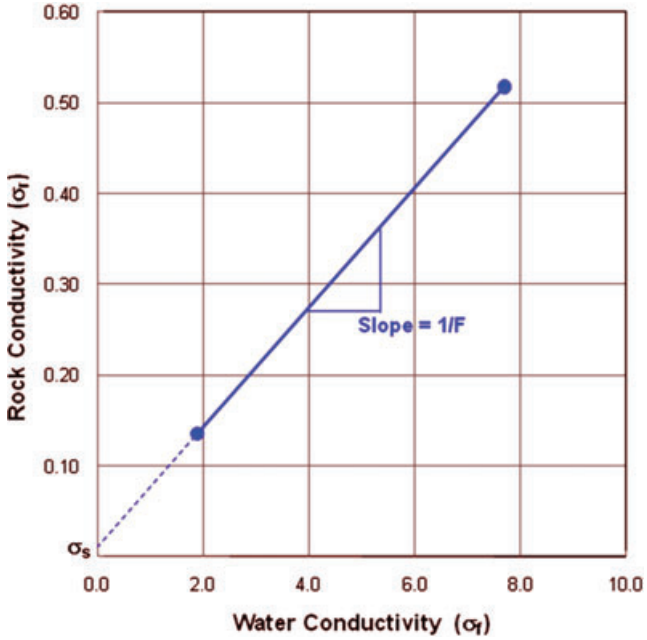

Figure 4. Determining the true formation factor '*F*' by plotting the measured rock conductivity 'σ_r' versus fluid conductivity 'σ_f'.

'F_M' (as defined by Stacey *et al.* 1960) varies from 1.013 to 1.034 (Table 1).

Plotting the magnetic lineation, foliation and magnetic anisotropy against height above the base of the sequence, reveals a similarity between the magnetic foliation and anisotropy curves, with no contribution from the magnetic lineation (Fig. 5). This plotting ensures that the magnetic pore foliation is the main contributor of the pore magnetic anisotropy.

As stated by Nabawy *et al*. (2009a), plots of the maximum and minimum magnetic pore susceptibility directions on equal area lower hemisphere stereographs show a clustering of the minimum axes around the vertical axis and clustering of the maximum pore elongation (maximum magnetic susceptibility) along the bedding plane close to the NE–SW or the NW–SE directions. Adindan and Kesieba formations at the base and top of the Nubia sandstones, respectively, show pore elongation varying between NNW and NW directions.

At the middle of the section, the pore fabric elongation for Abu Simbil Formation shows more scattering with the main direction referring to the NE direction.

Plotting the maximum magnetic susceptibility (χ'_{mag}) for Abu Ballas Formation shows differences from that of the other formations. The pore elongation is mainly clustered around the E–W direction, which is the main trend of the dominant faults in south Egypt, for example, Issawi (1978), Mousa (1984), Thabit (1994) and El-Sorady & Abdallah (2001).

3.2 Permeability measurements

We recall the results obtained for the permeability by Nabawy *et al*. (2009a). The magnetic pore fabric studies give the directions of the maximum, intermediate and minimum magnetic susceptibility. The first direction is perpendicular to the bedding plane, whereas the second and the third directions are parallel to the bedding plane. The average bulk permeability values range from 109.3 md at the top of Abu Simbil Formation to 7030 md in Abu Ballas formation with average 2463.3 md. According to Levorsen's classification (1967) of permeable reservoir rocks, the Nubia sandstones could be ranked as very good permeable rocks (Table 2). Due to the load pressure effect on sedimentary rocks, permeability values are expected to be higher along the bedding plane direction than in directions perpendicular to the bedding plane.

However, from the petrophysical study, some samples (Ad 3, Am 2, Abs 3 and Abs 5) show permeability values in the vertical direction (perpendicular direction to the bedding plane) higher than that measured horizontally, which could be attributed to permeable fracture porosity in the vertical direction.

Table 1. Magnetic pore fabric data for the studied Nubia sandstones (Nabawy *et al.* 2009a).

Formation	Site	Height (m)	λ_M	L_M	F_M	$Ø_{Fe}$
Kesieba Formation	Ks 3	240.5	1.034	1.003	1.031	23.2
	Ks 2	235.5	1.019	1.002	1.017	23.4
	Ks 1	228.0	1.029	1.004	1.024	19.8
Abu Ballas Formation	Abs 6	219.0	1.027	1.004	1.023	33.3
	Abs 5	214.0	1.024	1.002	1.021	30.1
	Abs 4	209.0	1.017	1.004	1.013	30.5
	Abs 3	204.0	1.020	1.003	1.017	22.9
	Abs 2	194.0	1.036	1.003	1.033	31.3
	Abs 1	175.5	1.020	1.003	1.017	26.9
Abu Simbil Formation	Am 7	165.5	1.024	1.003	1.021	34.1
	Am 6	150.5	1.035	1.003	1.032	23.2
	Am 5	136.0	1.028	1.002	1.026	31.9
	Am 4	124.5	1.036	1.002	1.034	22.0
	Am 3	83.5	1.019	1.003	1.017	30.0
	Am 2	73.0	1.018	1.004	1.015	24.7
	Am 1	70.0	1.034	1.010	1.024	29.2
Adindan Formation	Ad 3	41.5	1.024	1.003	1.022	20.7
	Ad 2	28.0	1.017	1.003	1.014	23.8
	Ad 1	2.50	1.029	1.002	1.027	25.9

Notes: λ_M is the magnetic pore anisotropy degree, L_M is the magnetic lineation, F_M is the magnetic foliation and $Ø_{Fe}$ (per cent) is the porosity measured by ferrofluid injection.

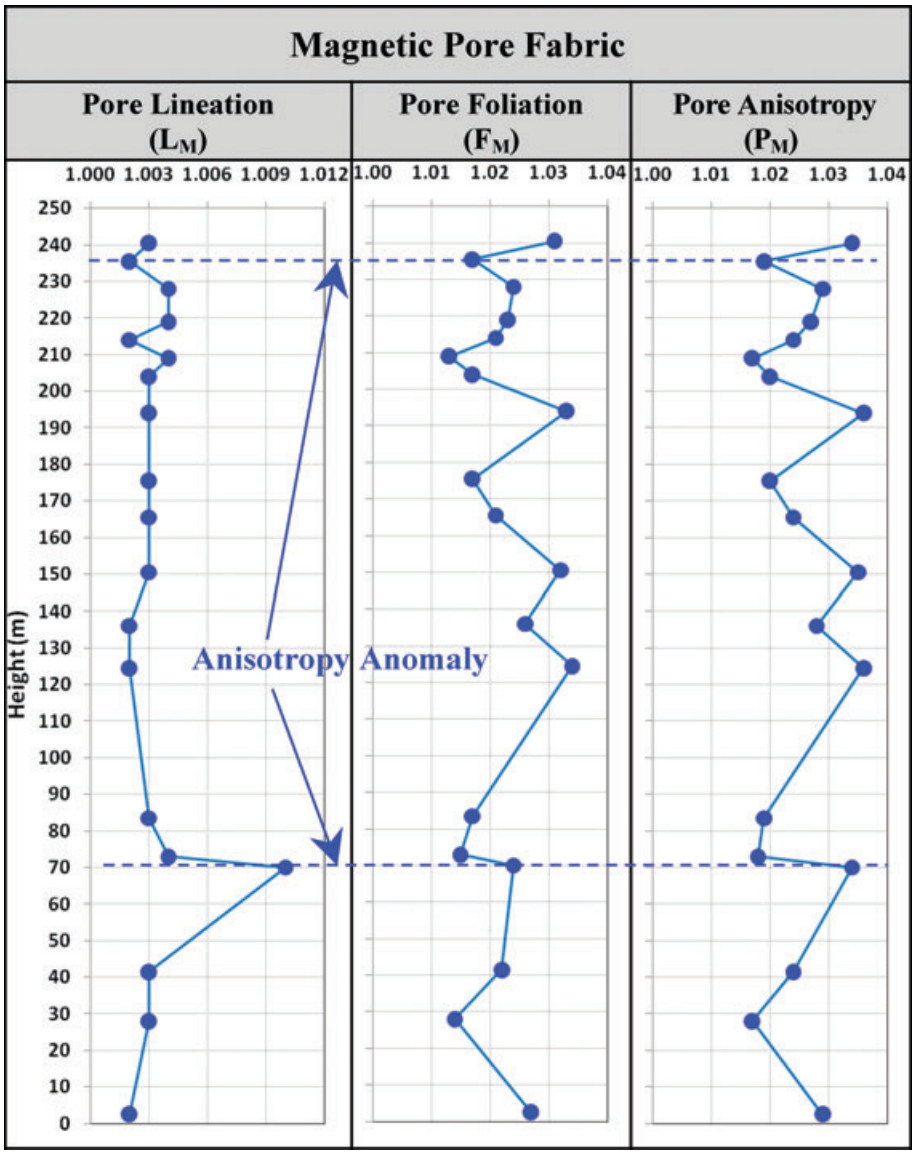

Figure 5. Vertical matching and correlating the anisotropy parameters of the magnetic pore fabric of the Nubia sandstones, south Egypt (Nabawy *et al.* 2009a).

For both Adindan and Kesieba Formations, the permeability values are the highest in the NW–SE direction. These directions are also obtained for the magnetic pore fabric maxima. On the other hand, the measured values for Abu Simbil Formation refer to the NE–SW direction with no distinct direction for Abu Ballas Formation. This could be explained by the structural patterns detected in Abu Ballas Formation, which has been exposed to many tectonic events. These events separated it from the underlying Abu Simbil Formation and caused the removal of the overlying Sabayia Formation from many places in the area of study in south Egypt. They brought also the Kesieba Formation in disconformity position with Abu Ballas.

3.3 Electric pore fabric

To compare the previous pore fabric results with electrical data, electrical resistivity and formation factor measurements have been carried out on oriented samples as described in Fig. 3. Data for the true formation factor and the electric fabric parameters are listed in Table 3.

Petrophysically, it is not easy to discriminate the studied samples into formations or facies, as they were similar in their electric properties. Accordingly, they were processed as one thick petrophysical facies.

Louis *et al*. (2003) compared the electric, magnetic and acoustic properties of several sandstone samples and concluded that, the nature of anisotropic behaviour of the Bentheim sandstone is mainly related to the pore shape anisotropy. The present samples are highly porous. Therefore, the electric fabric of the brine fully saturated samples and the obtained magnetic pore fabric of ferrofluid fully saturated samples are likely to result from the anisotropy of the pore shape.

Porosity values ($ø_W$) varies from 19.5 at the top parts of Abu Ballas Formation up 32.5 per cent at the top of Abu Simbil Formation which contains the most porous samples (Table 3).

Values of the true formation resistivity factor vary from 7.9 in the 30–120° direction to 76.3 in the 120–300° direction (Table 3).

The maximum true formation resistivity factors (F) were detected along the vertical directions for only one-third of the studied samples, whereas the maximum values for the other samples were

Table 2. Permeability values measured for the studied Nubia sandstones in the different directions (Nabawy *et al.* 2009a).

Formation	S. No.	k_V	k_{NE}	k_{NW}	k_b
Kesieba Formation	Ks 3	81.5	530.9	14.7	209.0
	Ks 2	2413.1	2564.9	4123.7	3033.9
	Ks 1	4800.2	4969.2	7750.0	5839.8
	Mean	**2431.6**	**2688.3**	**3962.8**	**3027.6**
Abu Ballas Formation	Abs 6	155.2	203.6	166.4	175.1
	Abs 5	3322.4	2980.2	2783.2	3028.6
	Abs 4	324.0	1161.0	1198.2	894.4
	Abs 3	1632.5	1258.8	1135.6	1342.3
	Abs 2	2154.0	5012.6	3628.4	3598.3
	Abs 1	4410.4	3736.3	4484.2	4210.3
	Mean	**2795.6**	**3026.1**	**2869.4**	**2208.2**
Abu Simbil Formation	Am 7	529.4	1706.3	1090.2	1108.6
	Am 6	33.9	154.2	139.8	109.3
	Am 5	432.4	615.2	674.0	573.9
	Am 4	589.6	723.0	698.2	670.3
	Am 3	2694.8	2736.9	2476.6	2636.1
	Am 2	2990.2	2890.8	1432.7	2437.9
	Am 1	4406.4	7008.0	5334.6	5583.0
	Mean	**1668.1**	**2262.1**	**1692.3**	**1874.2**
Adindan Formation	Ad 3	388.8	263.8	217.3	290.0
	Ad 2	1516.3	1653.4	1872.5	1680.7
	Ad 1	2285.7	2732.2	2561.0	2526.3
	Mean	**1396.9**	**1592.7**	**1550.3**	**1499.0**

Notes: kv (md) is the measured petrophysical permeability of the studied samples cored in a direction perpendicular to the bedding plane, k_{NE} (md) for samples cored parallel to the bedding plane in the NE direction, k_{NW} (md) for samples cored parallel to the bedding plane in the NW direction and k_b (md) is the average bulk permeability.

Table 3. True formation resistivity factors of the Nubia sandstones in south Egypt measured through the different directions accompanied with their electric fabric parameters.

Formation	S. No.	Height (m)	True formation factor (F)										
			F_{0-180}	F_{30-210}	F_{60-240}	F_{90-270}	$F_{120-300}$	$F_{150-330}$	F_P'	L_E	F_E	λ_E	$Ø'_W$
Kesieba Formation	Ks 3	240.5	36.76	27.62	12.66	28.90	28.99	27.62	27.93	2.15	1.35	1.70	21.77
	Ks 2	235.5	—	34.97	46.73	33.00	29.50	63.69	37.04	1.38	1.56	1.47	21.89
	Ks 1	228.0	28.99	10.92	46.51	31.75	8.39	35.21	35.34	3.36	1.65	2.35	21.47
Abu Ballas Formation	Abs 6	219.0	15.20	7.97	24.10	17.61	27.10	19.53	25.52	2.46	1.38	1.84	29.46
	Abs 5	214.0	20.08	21.88	30.40	25.38	24.81	20.49	37.74	1.29	1.46	1.37	28.87
	Abs 4	209.0	39.22	46.73	18.90	23.87	36.23	18.62	33.00	1.66	1.51	1.58	26.41
	Abs 3	204.0	—	27.40	51.02	—	18.66	32.79	30.58	1.72	1.59	1.65	29.52
	Abs 2	194.0	20.96	16.78	21.32	20.79	19.42	20.79	23.15	1.22	1.13	1.17	28.42
	Abs 1	175.5	26.25	13.35	16.26	19.16	16.08	22.17	18.42	1.41	1.40	1.40	29.52
Abu Simbil Formation	Am 7	165.5	19.49	23.04	16.03	20.00	20.88	20.00	23.31	1.27	1.14	1.21	32.48
	Am 6	150.5	25.13	28.99	28.01	26.27	25.45	24.69	27.40	1.08	1.09	1.08	25.58
	Am 5	136.0	19.05	14.08	26.25	19.96	20.08	25.25	29.59	1.57	1.34	1.45	31.17
	Am 4	124.5	36.50	28.99	26.70	36.10	31.75	66.67	45.66	1.46	1.71	1.58	21.16
	Am 3	83.5	9.01	22.78	24.39	9.62	31.25	16.84	21.19	2.14	1.62	1.86	27.86
	Am 2	73.0	22.42	31.25	30.21	25.91	52.91	20.16	29.94	1.51	1.74	1.62	23.06
	Am 1	70.0	15.15	15.24	16.08	20.08	21.60	21.88	21.65	1.24	1.16	1.20	26.68
Adindan Formation	Ad 3	41.5	30.30	40.32	31.35	35.34	30.86	34.36	35.34	1.12	1.19	1.15	22.77
	Ad 2	28.0	19.27	18.18	18.15	19.88	20.16	16.50	23.81	1.18	1.23	1.20	28.35
	Ad 1	2.5	26.56	41.49	24.94	69.93	76.34	25.58	35.21	1.72	1.78	1.75	24.76
		Average	24.14	24.84	26.84	26.86	28.45	28.04	29.57	1.63	1.42	1.51	25.55
		Minimum	9.01	7.97	12.66	9.62	8.39	16.50	18.42	1.08	1.09	1.08	19.46
		Maximum	39.22	46.73	51.02	69.93	76.34	66.67	45.66	3.36	1.78	2.35	32.48

Notes: $F_{P'}$ is the true formation factor average measured through the direction perpendicular to the bedding plane for the measured cubes (F_{P1}, F_{P2} and F_{P3}). F_{0-180}, F_{30-210}, F_{60-240}, F_{90-270}, $F_{120-300}$ and $F_{150-330}$ are the formation factors measured through the N–S, NNE–SSW, ENE–WSW, E–W, ESE–WNW and SSE–NNW directions, respectively. L_E, F_E and λ_E are the electric lineation, foliation and anisotropy values, respectively. $Ø'_W$ (per cent) is the water porosity average values for the measured cubes from each block sample.

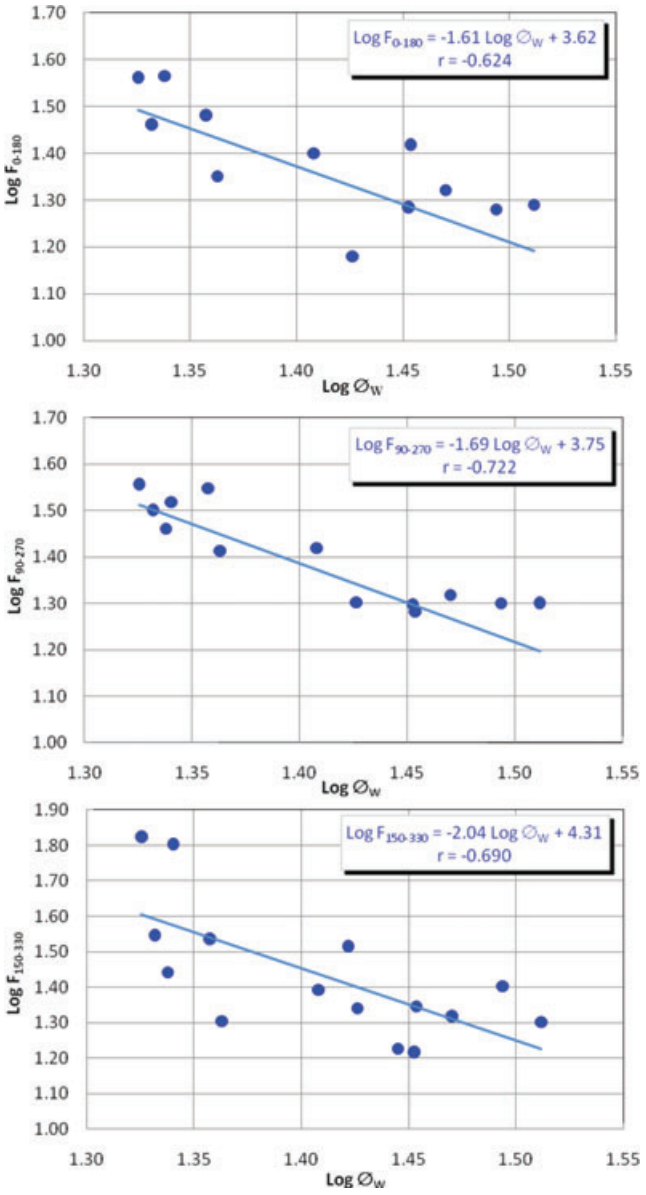

Figure 6. Plotting the log of true formation resistivity factor measured through the different horizontal directions oriented according to the magnetic north versus the log of porosity values measured by water injection.

scattered along the horizontal directions. On the other hand, the minimum F values (indicator for the pore elongation) are scattered among the different horizontal and the vertical directions with two-thirds of the lowest values recorded along the 0–180°, 30–210° and 150–330° directions, that is, fluctuating around the N–S direction.

The true formation resistivity factor (F) measured along the different horizontal directions is plotted against porosity in Fig. 6. Porosity $ø_W$ could be related to the formation resistivity factor measured in the 0–180° ($r = -0.624$), 90–270° ($r = -0.722$) and 150–330° ($r = -0.690$), whereas it is not likely related to F in the other directions ($-0.491 \leq r \leq 0$).

$$F_{0-180} = 3.62/\emptyset_W^{1.61} \qquad (r = -0.624), \tag{12}$$

$$F_{90-270} = 3.75/\emptyset_W^{1.69} \qquad (r = -0.722), \tag{13}$$

$$F_{150-330} = 4.31/\emptyset_W^{2.04} \qquad (r = -0.690). \tag{14}$$

These results could be explained by an elongation of the interconnected pore spaces in these directions that fluctuate around the N–S and the E–W, that is, more contribution for the measured porosity is coming from this direction.

Values of the lithology factors 'a' for the E–W, N–S and NNW–SSE directions are very close ranging between 3.62 and 4.31. This may be due to the siliceous sandstone composition of the studied rock samples. However, the obtained close values for both (a) and (m) constants indicate a high level of consistency of the obtained results along the different directions.

In general, two directions could be found in which the formation resistivity factors are dependent on and contributed mainly by the total pore spaces, that is, the electric fabric parameters for the present rocks are mainly due to the pore nature in these two perpendicular directions (N–S and E–W).

Similarly, values of the formation resistivity factor in the vertical direction (F'_p) are plotted against porosity values in Fig. 7, where porosity values could be related to the vertical true formation resistivity factor.

$$F'_p = 3.35/\emptyset_W^{1.35} \qquad (r = -0.758). \tag{15}$$

The average bulk formation factor (F′) was then plotted against the $ø_W$ in Fig. 8 where the average formation factor can be calculated in terms of the porosity values using the following equation:

$$F' = 3.37/\emptyset_W^{1.40} \qquad (r = -0.753). \tag{16}$$

The obtained equation shows (a) and (m) values similar to that obtained along the horizontal and vertical directions.

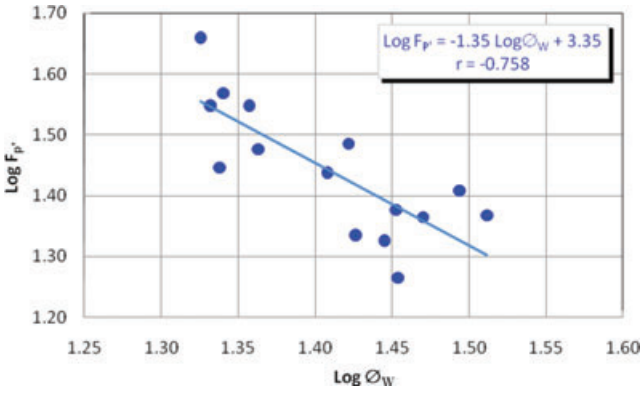

Figure 7. Plotting the log of porosity ($Ø_W$) measured by water injection plotted versus the log of true formation resistivity factor measured in a direction perpendicular to the bedding plane.

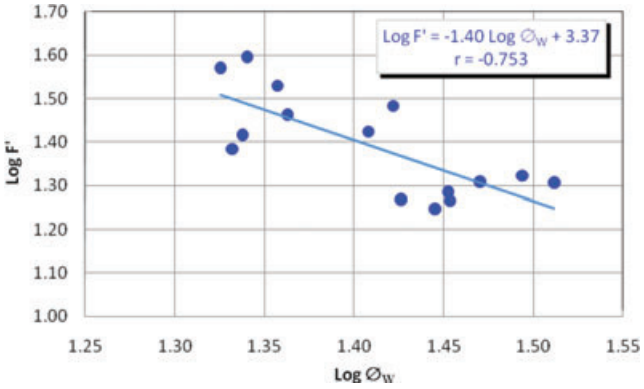

Figure 8. Plotting the log of porosity ($Ø_W$) measured by water injection versus the log of the overall average true formation resistivity factor.

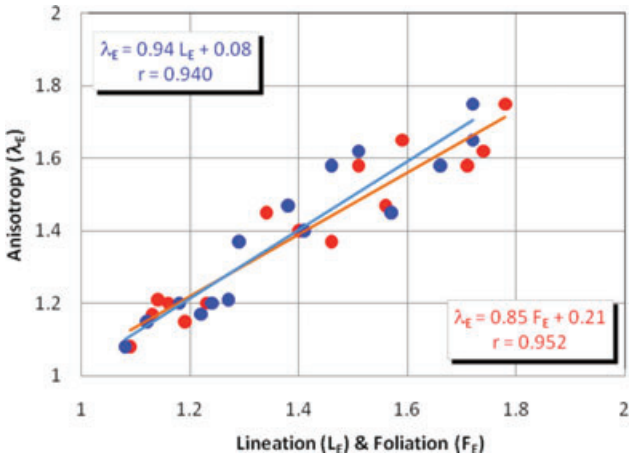

Figure 9. Plotting the electric anisotropy (λ_E) versus the electric lineation (L_E) and foliation (F_E) of the studied sandstone samples.

The electric pore fabric parameters (Table 3), on the other hand, vary from 1.08 to 3.36, from 1.09 to 1.78 and from 1.08 to 2.35 for the electric lineation (L_E), foliation (F_E) and anisotropy (λ_E) values calculated using the true formation factor. The electric fabric values of the studied rocks are ranked as slightly to moderately lineated, and slightly to moderately foliated fabrics. Therefore, the present rocks are ranked as slightly to moderately anisotropic (Nabawy & El-Hariri 2008).

The electric anisotropy values (λ_E) of the studied samples were plotted against their electric lineation (L_E) and foliation (F_E) as in Fig. 9. This plot reveals a dependence of the electric anisotropy (λ_E) on both the electric lineation (L_E) and foliation (F_E). This indicates a 3-D anisotropic ellipsoid shape of the obtained pore fabric.

$$\lambda_E = 0.94\ L_E + 0.08 \qquad (r = 0.940), \tag{17}$$

$$\lambda_E = 0.85\ F_E + 0.21 \qquad (r = 0.952). \tag{18}$$

On the other side, a relationship of relatively low correlation coefficient could be assigned between the electric lineation and foliation.

A comparison between the plots of L_E, F_E and λ_E against height evolution (Fig. 10) shows comparable peaks and anomalies at the different levels. Three peaks of anisotropy's anomalies could be recognized, at the base of the section in Adindan Formation, at the lower parts of Abu Simbil Formation at elevation 70.0 m and at the base of Kesieba Formation at the top parts of the section.

The anisotropy anomalies of the electric fabric, in general, could be used for tracing and comparing the Nubia sections in the different sites in the area of study.

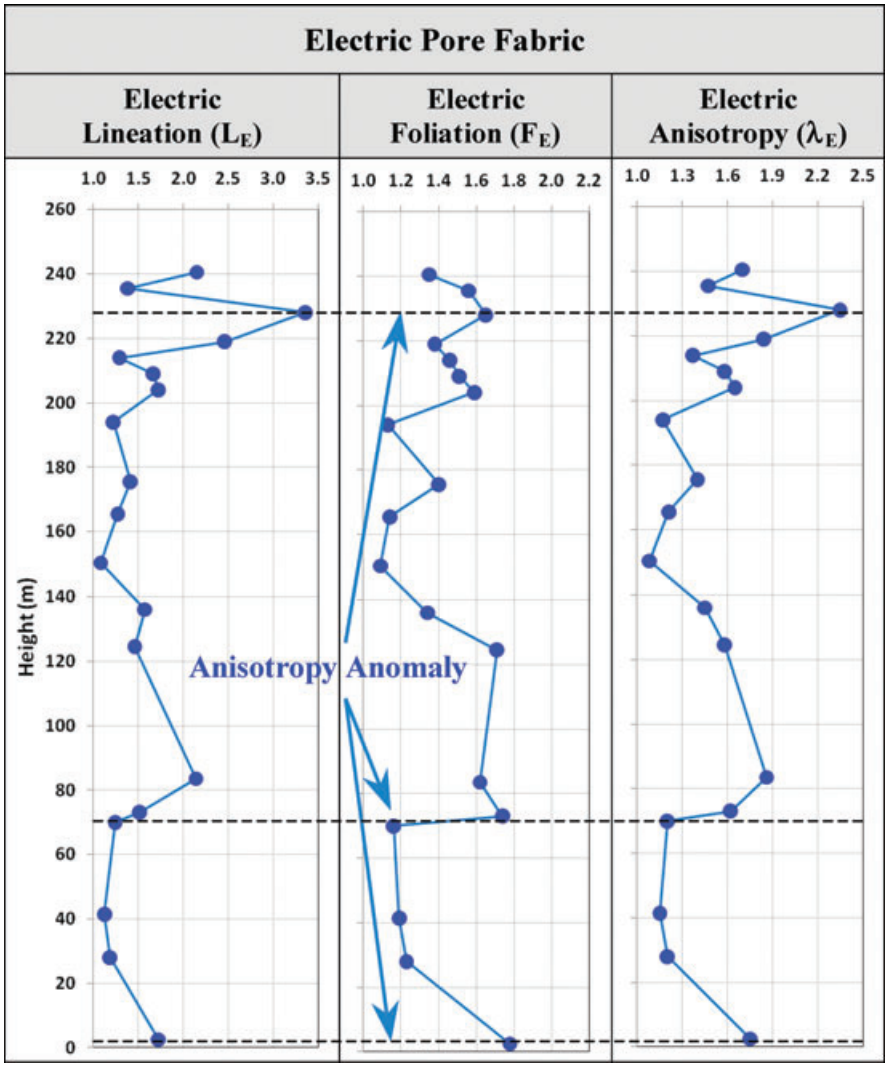

Figure 10. Vertical matching and correlation of the electric pore fabric parameters derived from the true formation factor of the Nubia sandstones.

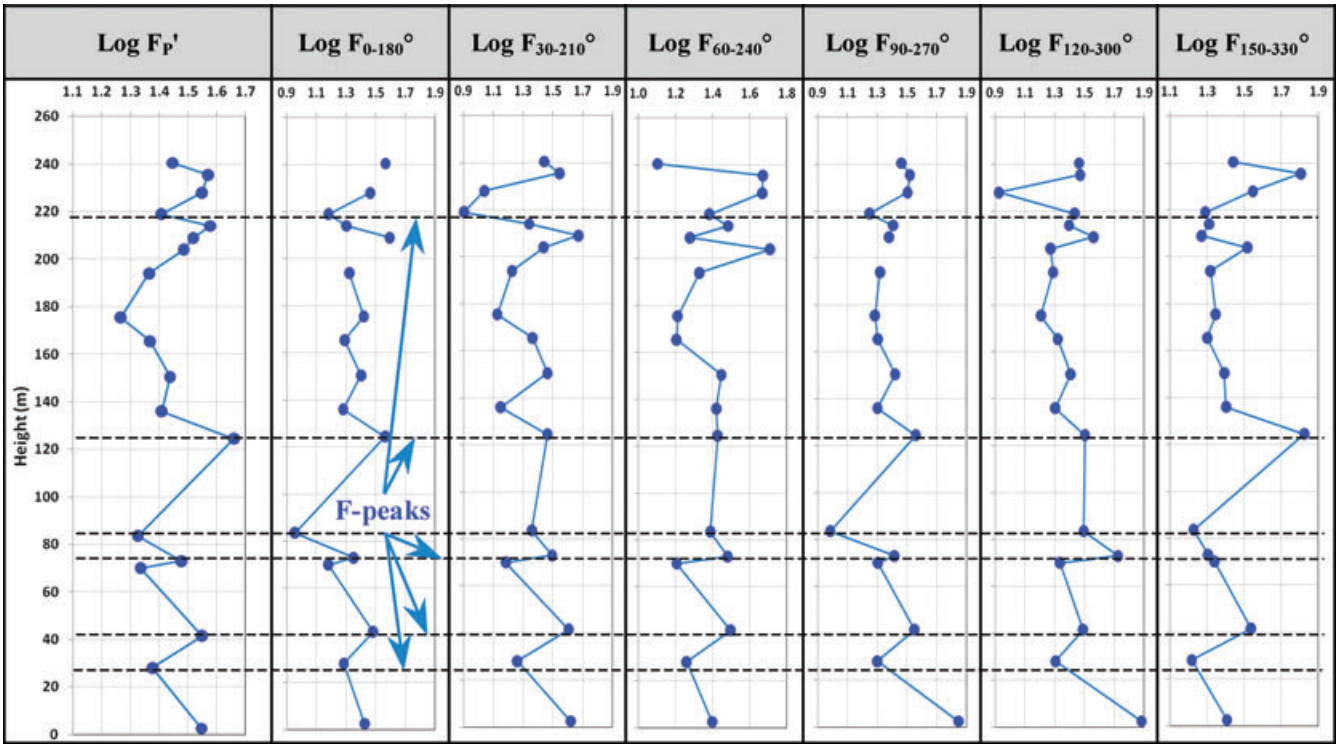

Figure 11. Vertical matching of log the true formation resistivity factors of the Nubia sandstones through the different directions. Denotations as in Table 3.

Plotting the true formation resistivity factor versus height (Fig. 11) indicates values common for porous sandstones. Some recorded formation resistivity peaks could be used for the horizontal tracing of the studied section in south Egypt.

4 GENERAL DISCUSSION

An electric fabric has been obtained for our highly porous samples. The observed electric fabric is likely correspondent to pore fabric. Using the electric pore fabric obtained from processing the true formation factor is recommended to avoid the influence of surface conductivity.

Measuring minimum F-values along the vertical directions and maximum F-values along the horizontal directions could be attributed to two reasons: (1) The presence of a crack system playing a sensitive rule in the electrical resistivity pattern of the studied samples and (2) the presence of some electrically active clay content. The independence of the formation resistivity factor on the nature of the pore spaces along some horizontal directions may be due to the complexity of pore distribution in these directions and their low contribution in the total volume of pore spaces. The cementation exponent (m) measured for F_P is relatively low which assigned for the highly porous rocks and may be due the presence of some clay content and/or vertical pathways/cracks. The lithology factor (a) is close to that obtained for the horizontal F factors, which could also be related to the homogeneity in the mineralogical composition of the studied samples.

The dependence of electrical resistivity of the fully saturated sandstones on porosity is more sophisticated than its dependence on stress due to compression, for example, in Brace & Orange (1968), Daily & Lin (1985), Lockner & Byerlee (1985) and Kaselow & Shapiro (2004). However, the effect of structural compression on the electrical resistivity of the Nubia sandstones is limited by their highly porous nature. It is limited to the grain cracking and to the grain-to-grain relation (Figs 2B and D).

A relationship of relatively low correlation coefficient could be assigned between the electric lineation and foliation indicating different origins for both. The relatively low electric foliation is mostly contributed by the load pressure, whereas the lineation is attributed to later fracture system.

A comparison between the plots of L_E, F_E and λ_E against height evolution (Fig. 10) shows comparable three peaks of anisotropy's anomalies at the different levels. The first and second peaks at the base of Adindan and Abu Simbil Formations may be related to the load pressure effect accompanied with some cracks on the grain scale (Figs 2A and B).

The third beak at the base of Kesieba Formation can be attributed to electric lineation due to some tectonic events that led to a fracture system. This could be ensured by the fact that Kesieba Formation was preceded by a somewhat long history of tectonism causing erosion and releasing of the underlying Sabayia Formation, which caused a disconformity between the underlying Abu Ballas Formation and the overlying Kesieba Formation.

Conducting the present electric technique on the studied samples revealed two consistent directions assigned as preferred directions for the fluid migration paths, one swinging to the N–S direction and the other swings to the E–W which are consistent with the magnetic pore fabric.

A discrepancy between the electric and magnetic pore fabric technique reveals some minimum resistivity values (direction of pore elongation) along the vertical direction (compare Tables 1 and 3) and instead some maximum resistivity values along the horizontal plane which is not the case with the magnetic fabric technique.

So, a question can be raised: Is the brine solution used for the electric fabric assignment more invasive than the ferrofluid used for the magnetic pore fabric? Therefore, porosity obtained from injection of both fluids ($Ø_{Fe}$ & $Ø_W$) was plotted together against

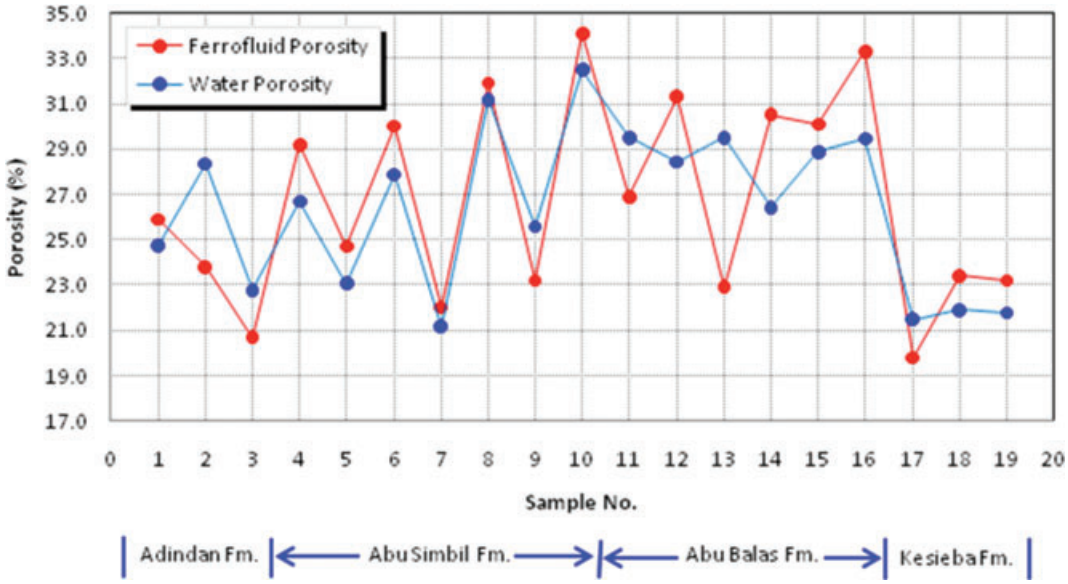

Figure 12. Correlation chart between porosity values measured by ferrofluid and brine injection techniques.

the samples numbers (Fig. 12), which indicates a higher ferrofluid porosity ($Ø_{Fe}$) for 74 per cent of the studied samples. This ensures higher invasion ability for the ferrofluid than the saline solution, where the size of the ferrofluid molecules is ranging between 1nm and 10 nm and not affected by the swelling property of the clay minerals.

Therefore, the present discrepancy can be explained by the fact that, the magnetic pore fabric technique can assign the pore volume and its frequency distribution but can't detect cracks. On the other hand, the electric pore elongation refers to the easiest way in which the electric current can go through, that is, can easily detect cracks. Cracking is usually acting in vertical and/or inclined directions causing increasing the permeable paths vertically and reducing the electrical resistivity values in the vertical direction to the minimum values.

However, a general matching of the output main pore elongation and lineation trends obtained from the electric pore fabric technique, the magnetic pore fabric and from measuring permeability in 3-D have been listed in Table 4.

A similarity between pore fabrics are obtained for 28 per cent of the studied samples using the three techniques, and for 66.7 per cent of the samples using the both electric pore fabric and 3-D permeability.

In general, it is thought that the electric pore fabric technique is a successful technique that could be used for assigning the preferred permeable paths for fluid migration.

5 MODELLING TRANSPORT PROPERTIES THROUGH THE PORE CHANNELS

There are many trials related to the assignment of the main factors controlling transport through pore spaces following Poiseuille's law to simulate the pore spaces as long tubes of circular cross sections. The intent of this trial is to focus on creating a new model with reasonable structures and high reliability. Although the pore spaces are ellipsoidal in cross section, some facts to be taken into consideration may lead to more reliable simple simulation.

First, the pore throat apertures, not the pore volume, control transportation through the pore channels. In addition, the velocity of the current flow through the pore channels increases towards the middle parts of the pore space and decreases in the pore wall direction. Moreover, presence of some clay content and other authigenic minerals tend to line the pore space volume, that is, to decrease its curvature.

From this study, the magnetic pore foliation as an indicator for the elliptical cross section and pore volume, ranges between 1.013 and 1.034, that is, foliation of the pore volume as a whole is less than 3.4 per cent. On the other hand, it is noted petrographically that most of the macro pore spaces that control the fluid transportation are more or less circular in shape (Fig. 2D).

In general, the current flow properties, the nature of the pore wall and the effect of the authigenic minerals lead us to simulate the pore space as pore channel tubes of circular cross section. Therefore, on the samples scale, the permeability 'k' of a random network of pore channels of average pore radius 'r' and connected porosity 'Ø' could be assigned as follows (Guéguen, & Palciauskas 1994; Mavco *et al.* 2009):

$$k = \frac{r^2}{8} \times \phi. \tag{19}$$

On the other hand, the formation resistivity factor is related to the pore volume using Archie's law (1942)

$$F = a\phi^{-m}. \tag{20}$$

Therefore, the permeability can be calculated in terms of 'F' and 'r' as follows:

$$k = \frac{r^2}{8} \times \left(\frac{a}{F}\right)^{\frac{1}{m}}, \tag{21}$$

where, 'k' and 'r' are measured in μm and 'r' could be obtained from the mercury injection tests.

The total pore volume determined from mercury injection tests '$Ø_{Hg}$' is mostly higher than that obtained using the water injection '$Ø_W$' which controls the formation factor. This can be related to the presence of some micropore spaces, which are accessible to the mercury injection at high pressure but not for the water injection

Table 4. A comparison between directions of the maximum pore lineation obtained by the different used techniques.

Formation	S. No.	Elevation (m)	Direction of True F_{min}	Direction of χ_{max}	Direction of k_{max}
Kesieba Formation	Ks 3	240.5			
	Ks 2	235.5			
	Ks 1	228.0			
	Dominant direction				
Abu Ballas Formation	Abs 6	219.0			
	Abs 5	214.0			
	Abs 4	209.0			
	Abs 3	204.0			
	Abs 2	194.0			
	Abs 1	175.5	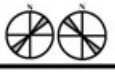		
	Dominant direction		----		----
Abu Simbil Formation	Am 7	165.5			
	Am 6	150.5			
	Am 5	136.0			
	Am 4	124.5			
	Am 3	83.5			
	Am 2	73.0			
	Am 1	70.0			
	Dominant direction				
Adindan Formation	Ad 3	41.5			
	Ad 2	28.0			
	Ad 1	2.50			
	Dominant direction				

at low pressure. Therefore, using 'r' obtained from the mercury injection is mostly representative for pore volume higher than that occupied during measuring the formation factor. So, eq. (13) should be adopted by a multiplication factor 'b' as follows:

$$k = b \times \left(\frac{r^2}{8} \times \left(\frac{a}{F} \right)^{\frac{1}{m}} \right) + c, \tag{22}$$

where, 'b' is a multiplication factor and 'c' is a constant; values of c and b depend on the difference between Ø_{Hg} and ø_{W}.

From this study, the average formation factor F' was calculated in terms of 'Ø_{W}' values with lithology factor 'a' and cementation exponent 'm' equal to 3.37 and 1.40 (eq. 16), respectively.

By substituting for 'a' and 'm' in the last equation we get

$$k = b \times \left(\frac{r^2}{8} \times \left(\frac{3.37}{F'} \right)^{0.71} \right) + c. \tag{23}$$

Nabawy *et al*. (2009b), studied the pore throat distribution of the Nubia sandstones and determined their corresponding pore radius 'r' distribution. They plotted the Hg saturation versus the Hg saturation divided by the applied pressure and defined a main apex of the obtained hyperbola at average value equals to 45.2 per cent Hg saturation and correspondent pore radius r_{apex} at 8.4 μm which is a representative average pore radius.

Using the r_{apex} and the average true formation factor data enabled us to calculate permeability in μm^2 with a high reliability. To check the reliability of the proposed model, the calculated k_c is plotted versus the measured k_m (Fig. 13).

Two sets of samples could be distinguished; each set follows a definite trend for the calculated and measured permeability with a very high reliability. For both sets, the constant 'c' is more or less similar, whereas the 'b' factor is the effective parameter.

The first set is characterized with $b < 1$ (corresponds to samples have a low difference between Ø_{Hg} and Ø_{W}), whereas for the other one $b > 1$ (corresponds to samples have a high difference between Ø_{Hg} and Ø_{W}). Therefore, the multiplication factor 'b' is dependent mostly on the present volume of micropore spaces, which is accessible for the mercury injection but not accessible for the brine solutions during the electric measurements.

Although 'r_{apex}' is a bulk average value, testing the proposed model for 'k' and 'F' measured through the vertical and horizontal directions indicates applicability of this model not only for the bulk sample but also along the different directions.

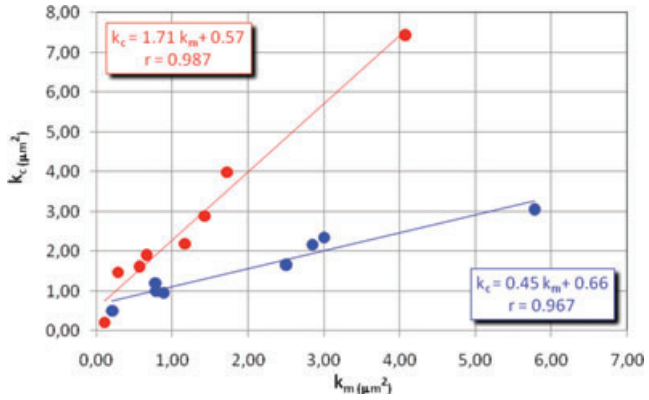

Figure 13. Plotting the calculated permeability (k_c) versus the measured bulk permeability (k_m).

6 CONCLUSIONS

The Nubia sandstones are highly porous quartz arenite similar in their petrophysical behaviour, so they were processed as one thick petrophysical facies. In general, the maximum true formation resistivity factors were detected mostly through the perpendicular directions, whereas the minimum values are scattered through the different horizontal and vertical directions. The highly porous rocks act electrically like a homogeneous medium and their obtained electric fabrics are raised mainly from the anisotropy of their pore shapes.

The electric pore fabric is ranked as slightly to moderately anisotropic fabrics raised mainly from the electric foliation.

Conducting the electric pore fabric technique revealed two consistent directions, which were assigned as preferred directions for the fluid migration paths, one swinging to the N–S direction and the other refers to the E–W.

Applying the magnetic pore fabric technique can easily define the pore elongation but cannot detect cracks which form negligible part of the total pore volume. On the other side, the electric fabric technique refers to the easiest way in which the electric current can go through, that is, the shortest one. It can easily detect cracks rather than the pore elongation.

The highly porous nature of the present rocks may limit the efficiency of the present technique by giving rise to low to very low electrical resistivity values with negligible differences.

Directions of the maximum permeability obtained from the 3-D measurements could be easily related to the directions of the electric pore lineation rather than the magnetic one.

The authors believe that, the efficiency of the present technique could be increased by more permeability measurements in additional directions.

ACKNOWLEDGMENT

The authors thank Profs Yves Gueguen and Christian David for their peer review and great comments that improved and reconstructed the manuscript. Thanks are also due to the editor Prof. Mark Everett whose patience and insightful suggestions have led to a new concise revised version. The experimental work in Aix-en-Provence and Strasbourg was supported by the Imhotep Hubert Curien programme, and final writing performed thanks to a grant from Ville de Paris.

REFERENCES

Amyx, J.W., Bass, D.M. & Whiting, R.L., 1960. *Petroleum Reservoir Engineering: Physical Properties*, McGraw-Hill Book Company Incorporation, London.

Archie, G.E., 1942. The electric resistivity logs as an aid in determining some reservoir characteristics, *Trans. Am. Int. Mech. Eng.*, **146**, 54–62.

Balsley, J.R. & Buddington, A.F., 1960. Magnetic susceptibility anisotropy and fabric of some Adirondack granites and orthogneisses, *Am. J. Sci.*, **258A**, 6–20.

Brace, W. & Orange, A., 1968. Electrical resistivity changes in saturated rocks during fracture and frictional sliding, *J. geophys. Res.*, **73**, 1433–1445.

Daily, W. & Lin, W., 1985. Laboratory-determined transport properties of Berea sandstone, *Geophysics*, **50**, 775–784.

EGPC-CONOCO, 1987. Geological Map of Egypt, NF 36 NW, *ElSaad ElAli*, **1**, 500 000.

El-Sorady, A.I. & Abdallah, A.A., 2001. Geotechnical studies on the area of new Tushka city, *Ann. Geol. Surv. Egypt*, **xxiv**, 521–539.

Glover, P.W.J., Gomez, J.B., Meredith, P.G., Boon, S.A., Sammonds, P.R. & Murrell, S.A.F., 1996. Modelling the stress-strain behavior of saturated

rocks undergoing triaxial deformation using complex electrical conductivity measurements, *Surv. Geophys.*, **17**, 307–330.

Glover, P.W.J., Gomez, J.B., Meredith, P.G., Hayashi, K., Sammonds, P.R. & Murrel, S.A.F., 1997. Damage of saturated rocks undergoing triaxial deformation using complex electrical conductivity measurements: experimental results, *Phys. Chem. Earth*, **22**, 57–61.

Guéguen, Y. & Palciauskas, V., 1994. *Introduction to the Physics of Rocks*, Princeton University Press, New Jersey, 294 pp.

Hamilton, N. & Rees, A.I., 1970. The use of magnetic fabric in palaeocurrent estimation, in *Palaeogeophysics*, pp. 445–464, ed. Runcorn, S.K., Academic Press, London.

Hendriks, F., 1987. Die Entwicklung sgeschichte des SE-Ägyptischen sedimentations raumes in der kreide und in Alttertiär: Eine Beckenstudie, unpubl., Habilschr., Tu Berline, 167 pp.

Hendriks, F., 1988. Evolution of the depositional environments of SE Egypt during the Cretaceous and Lower tertiary, *Bel. Geowiss. Abh.*, **75**(1), 49–82.

Hrouda, F., 1982. Magnetic anisotropy of rocks and its application in geology and geophysics, *Geophys. Surv.*, **5**(1), 37–82.

Issawi, B., 1973. Nubia sandstone type section, *AAPG Bull.*, **57**, 741–745.

Issawi, B., 1978. Geology of the Nubia west area, Western Desert, Egypt, *Ann. Geol. Surv. Egypt*, **8**, 237–253.

Issawi, B. & Jux, U., 1982. Contribution to the stratigraphy of Paleozoic rocks in Egypt, *Ann. Geol. Surv. Egypt*, **64**, 1–28.

Issawi, B. & Osman, R.A., 1993. Tectonic-Sedimentary synthesis of paleozoic-cretaceous clastics, SW Aswan, Egypt, *J. Sed. Egypt*, **1**, 11–22.

Jouniaux, L., Zamora, M. & Reuschlé, T., 2006. Electrical conductivity evolution of non-saturated carbonate rocks during deformation up to failure, *Geophys. J. Int.*, **167**, 1017–1026.

Kaselow, A. & Shapiro, S.A., 2004. Stress sensitivity of elastic moduli and electrical resistivity in porous rocks, *J. geophys. Eng.*, **1**, 1–11.

Klitzsch, E., 1979. Zur geologie des gilf kebir gebietes in der ostsahara, *Cla. Geol. Abh.*, **30**, 113–132.

Klitzsch, E. & Hermina, M., 1989. *The Mesozoic, in Stratigraphic Lexion and Exploratory Notes to Accompany the Geological Map of Egypt, 1:50000*. CONOCO Inc., Cairo, Egypt, 256 pp.

Lamb, H., 1945. Hydrodynamics. Dover, New York.

Levorsen, A.I., 1967. *Geology of Petroleum*, W.H. Freeman Company, San Francisco, ISBN 0716702304.

Lockner, D. & Byerlee, J., 1985. Complex resistivity measurements of confined rocks, *J. geophys. Res.*, **90**, 7837–7847.

Louis, L., David, C. & Robion, P., 2003. Comparison of the anisotropic behaviour of reservoir rocks under dry and wet conditions, *Tectonophysics*, **370**, 193–212.

Lynch, E.J., 1962. *Formation Evaluation*, Harper and Row Pub., New York, ISBN 0063562901.

Mavco, G., Mukerji, T. & Dvorkin, J., 2009. *The Rock Physics Handbook: Tools for Seismic Analysis of Porous Media*, 2nd edn, Cambridge Univ. Press, 511 p, ISBN 978-0-521-86136-6.

Mousa, M.F., 1984. interpretation of magnetic anomalies of the Aswan-Tushka area, Western Desert, Egypt, *M.Sc. Thesis*, Assuit Univ., unpublished, 132 pp.

Nabawy, B.S. & El-Hariri, T.Y., 2008. Electric Fabric of Subsurface Cretaceous Rock, Abu Gharadig basin, Western Desert, Egypt, *J. Afr. Earth Sci.*, **52**, 55–61.

Nabawy, B.S., Rochette, P. & Géraud, Y., 2009a. Petrophysical and magnetic pore network anisotropy of some cretaceous sandstone from Tushka Basin, Egypt, *Geophys. J. Int.*, **177**(1), 43–61.

Nabawy, B.S., Rochette, P., Géraud, Y. & Nicolas, B., 2009b. Pore-throat characterization in highly porous and permeable sandstones, *AAPG Bull.*, **93**(6), 719–739.

Olhoeft, G., 1989. Electrical properties of rocks, in: *Physical Properties of Rocks and Minerals*, pp. 257–329, ed. Touloukian, Y.S., Judd, W.R. & Roy, R.F., Hemisphere, New York.

Parkhomenko, E.I., 1982. Electrical resistivity of minerals and rocks at high temperature and pressure, *Rev. Geophys.*, **20**, 193–218.

Pfleiderer, S. & Kissel, C., 1994. Variation of pore fabric across a fold-thrust structure, *Geophys. Res. Let.*, **21/19**, 2147–2150.

Ragab, M.A., El Sayed, A.A. & Nabawy, B.S., 2000. Physical parameters of Egyptian oil reservoir sedimentary rocks, A review, in *Sedimentary Geology of Egypt, Applications and Economics*, pp. 129–150, ed Soliman, S.M., Sedimentological Society of Egypt, Cairo.

Said, R., 1962. *Geology of Egypt*, Elsevier Pub. Co., Amsterdam, New York.

Salem, H.S. & Chilingarian, G.V., 1999. The cementation factor of Archie's equation for shaly sandstone reservoirs, *J. Petrol. Sci. Eng.*, **23/2**, 83–93.

Serra, O., 1984. *Fundamentals of Well-Log Interpretation*, Elsevier, Amsterdam.

Stacey, F.D., Joplin, G. & Lindsay, J., 1960. Magnetic anisotropy and fabric of some foliated rocks from S.E. Australia, *Geophys. Pure. Appl.*, **47**, 30–40.

Tarling, D.H. & Hrouda, F., 1993. *The Magnetic Anisotropy of Rocks*, Chapman and Hall, London.

Thabit, G.K., 1994. Sedimentology of the Nubia group in the area southwest of Aswan, Abu Simbil area, unpublished, *M.Sc. Thesis*, Assuit Univ., 164 pp.

Wilt, M. & Alumbaugh, D., 1998. Electromagnetic methods for development and production: state of the art, *Leading Edge*, **17**, 487–490.

Winsauer, W.O., Shearin, H.M., Masson, P.H. & Williams, M., 1952. Resistivity of brine-saturated sands in relation to pore geometry, *AAPG Bull.*, **36/2**, 253–277.

Worthington, P.F., 1985. Evolution of shaley sand concepts in reservoir evaluation, *Log Analyst*, **26**, 23–40.

Wyllie, M.R.J. & Rose, W.D., 1950. Some theoretical considerations related to the quantitative evaluation of the physical characteristics of reservoir rocks from electric log data, *J. Petrol. Techno.*, **189**, 105–108.